The effect of ultrasonic irradiation on the microstructure and corrosion rate of a Zn – 4.8 wt.% Al galvanising alloy used in high performance construction coatings

James Sullivan, David Penney, Jonathan Elvins, Khalil Khan

PII: S0257-8972(16)30050-0
DOI: doi: 10.1016/j.surfcoat.2016.01.050
Reference: SCT 20898

To appear in: *Surface & Coatings Technology*

Received date: 31 October 2015
Revised date: 18 January 2016
Accepted date: 25 January 2016

Please cite this article as: James Sullivan, David Penney, Jonathan Elvins, Khalil Khan, The effect of ultrasonic irradiation on the microstructure and corrosion rate of a Zn – 4.8 wt.% Al galvanising alloy used in high performance construction coatings, *Surface & Coatings Technology* (2016), doi: 10.1016/j.surfcoat.2016.01.050

The effect of ultrasonic irradiation on the microstructure and corrosion rate of a Zn – 4.8 wt.% Al galvanising alloy used in high performance construction coatings

James Sullivan[a], David Penney[a], Jonathan Elvins[b], Khalil Khan[a]

[a] Materials Research Centre, College of Engineering, Swansea University Bay Campus, Fabian Way, Swansea, SA1 8QQ

[b] Tata Steel Europe, SPECIFIC, Baglan Bay Innovation Centre, Central Avenue, Baglan SA12 7AX

Corresponding author – Professor James Sullivan, Materials Research Centre, College of Engineering, Swansea University Bay Campus, Fabian Way, Swansea, SA1 8QQ

Email – j.h.sullivan@swansea.ac.uk

Tel - +44 1792 602495

Fax - +44 1792 295676

Abstract

The microstructure and corrosion resistance of a Zn – 4.8 wt.% Al alloy, typically used for high performance galvanised coatings for construction, was modified by the application of ultrasound during solidification. The alloy exposed to ultrasound had an increased volume fraction of smaller, discrete primary η Zn phase regions that were more uniformly distributed throughout the casting. The morphology of η Zn was altered from dendritic to globular and the Zn/Al eutectic growth was disrupted in localised areas from lamellar to anomalous. These changes were likely due to the physical action of the ultrasound disrupting compositional effects, fragmenting dendrites and through the development of cavitation events causing disruptive mixing. These microstructural changes produced an enhanced cut-edge corrosion resistance of the alloy in 0.1% NaCl when coupled with steel mimicking in service coating conditions that was investigated using the SVET. The primary η Zn crystal regions were focussed sites for anodic Zn dissolution and the smaller η regions produced by ultrasound reduced the corrosion rate by preventing the development of crevice like phenomena that may be associated with larger dendrites. The number and size of primary η Zn regions affected the corrosion rate with reductions in these factors reducing the corrosion rate of the alloy.

Keywords: Galvanising; Ultrasound; Zn-Al; Microstructure; Corrosion;

1.0 Introduction

Ultrasonic irradiation of solidifying alloys has been shown to have significant effects on the microstructure and mechanical properties of a range of important engineering alloys as shown previously [1-16]. ___. Ultrasound creates unique conditions within solidifying melts. The irradiation creates intense localised temperature and pressure fluctuations within the melt through cavitation events and the promotion of mixing through acoustic streaming. These conditions are thought to contribute to the change in microstructure observed when solidifying under such irradiation. Solidification under these conditions has been shown to dramatically influence the nucleation rate of phases within alloys and this has been attributed to a number of factors including dendrite fragmentation, pressure assisted nucleation, de-gassing of nucleants and uniform dispersal of nucleants [1-16]. In this work ultrasound has been used to irradiate a Zn - 4.8 wt.% Al alloy that is used extensively by Tata Steel Europe for the coating of steel through galvanising. This alloy is a development of the Galfan alloy coating that has a 5 wt.% Al addition and provides lifetimes of 30-40 years for premium coated steels for construction. The alloy coating acts to sacrificially protect the steel by corroding preferentially when exposed to the environment. When coupled to steel and exposed to an environment containing water and oxygen, the Zn in the coating anodically dissolves to form Zn^{2+} ions whilst the corrosion potential of the steel is cathodically polarised thus retarding its corrosion rate. The subsequent reaction of Zn^{2+} ions with anions from the cathodic reaction or surrounding environment form insoluble corrosion products that further reduce continued corrosion. The Al in the coating forms an adherent Al_2O_3 oxide that slows the rate of corrosion of the coating whilst retaining its sacrificial protection of the steel. This provides the coating with an additional lifespan over traditional Zn only galvanised coatings. After galvanising, the Zn – 4.8wt.% Al alloy coated steel is further coated with organic paint

layers to provide rapid build pre-finished steel for the construction sector and the general failure mechanism of these materials is organic coating delamination due to cut-edge corrosion of the galvanising alloy / steel couple. The Zn - 4.8 wt.% Al alloy solidifies as a two phase microstructure of primary Zn rich η dendrites and a Zn / Al lamellar eutectic under practical and production cooling rates. It has been previously demonstrated that control of the primary Zn η dendritic phase with regards to a reduced dendrite size and increased nucleation rate can offer improvements to the cut-edge corrosion resistance of the alloy [17] and thus it was hoped that ultrasonic irradiation on solidification may further enhance this due to increased nucleation of the primary Zn rich phase. Here, castings of this alloy have been solidified with and without ultrasonic irradiation and the microstructure and corrosion resistance of the alloy examined to assess the effects of the irradiation. A method has been developed to mimic a finished coated galvanised steel cut-edge of the material by inserting a steel bar into the casting post solidification in order to assess the sacrificial corrosion action of the alloy after ultrasonic irradiation.

2.0 Experimental

2.1 Ultrasonic irradiation

The ultrasonic irradiation experiments were performed at the Tata Steel, Galvanising line number six in Shotton, Deeside, UK. Graphite Crucibles of volume 250 ml were pre-heated in an oven to 100^{o}C and 140 ml (1kg) of Zn - 4.8 wt.% Al alloy was taken directly from the galvanising bath using a ladle and poured into the crucible. The temperature of the alloy in the ladle was 450^{o}C and the ladle was pre-heated through immersion in the bath to ensure solidification did not occur in the ladle. The ultrasound probe with a 13 mm diameter titanium horn was then lowered into the molten metal to a depth of approximately 5 mm below the melt line and held steady using a clamp stand as shown schematically in figure 1.

The ultrasonic horn was pre-heated to 100^{o}C using a blow torch and measured with an infrared thermometer prior to introduction to the melt in order to reduce cooling effects produced by the titanium horn. Ultrasonic irradiation at 20 kHz and an amplitude of 50 μm was then applied to the melt using the Branson Sonifier 250CE control unit for the transducer at the full power of the unit of 200W with no pulsing of the ultrasound to ensure 100% applied power during the cycle. The horn was gently moved laterally periodically to assess the condition of the melt and removed once a mushy / semi-solid state was achieved. This generally was within 90 seconds of the application of the molten metal to the crucible. The experiment was repeated with another crucible, molten metal added and the ultrasonic horn heated and lowered into the melt but this time no ultrasonic irradiation was applied in order to assess the control solidification behaviour of the alloy whilst replicating any cooling effect the introduction of the horn may have had. After solidification and cooling had completed the casts were removed from the crucibles and sectioned in half. The sections were then polished on the cut face to a metallographic finish to enable the microstructure of the alloy to be assessed at various depths through the casting directly below ultrasonic horn.

2.2 Analysis of microstructures

The cut face of each section of casting was polished to a 1 μm metallographic finish using progressively finer emery papers and diamond slurry. The section was then etched using 1% Nital and an example of such sectioned cast samples with ultrasonic irradiation is shown in figure 2A. The structure of the cast samples were then analysed initially macroscopically with digital images taken using a Nikon Coolpix digital camera mounted on a height adjustable gantry. Microstructures were then assessed using a MEF3 Reichert optical microscope at a variety of magnifications. To assess the morphology and volume fraction of phases, images at 20 times magnification were taken at 5 mm increments from the location of the bottom of the

ultrasonic horn down the centre of the casting to a distance of 40 mm from the horn as shown in figure 2A. To quantify the primary phase volume fraction image analysis software, JSAC Paint Shop Pro X, was used to colour the primary phase white in each image. Sigmascan Pro 5 software was then used to calculate the area of primary phase per image to provide an instantaneous volume fraction associated with solidification at that point in the casting. In order to examine the finer morphology of the primary and eutectic phases images were taken at times 100 magnification using the Reichert optical microscope. EDX analysis of the microstructures and post corrosion attack was examined using a Hitachi TM3000 Bench top SEM. To confirm the phases present in the microstructures XRD analysis was carried out using a Bruker D8 Discover Diffractomer using a Cu Kα radiation (λ = 0.15406nm) source. Samples were subjected to cycle with parameters of 0.5 seconds per step and 0.0006^{o} increments per step between 5 and 80^{o}.

2.3 Assessment of corrosion behaviour using the Scanning Vibrating Electrode Technique (SVET)

The Zn - 4.8 wt.% Al alloy used in this investigation is not used as bare coated galvanised product and in service it is always over coated with organic coatings. Therefore, the failure mechanism is always down to cut-edge corrosion rather than surface corrosion. At a cut-edge the coupled system of Zn – 4.8 wt.% Al alloy coating and steel is exposed to the environment and thus the coating corrodes preferentially to protect the steel substrate through cathodic protection. In order to assess the castings produced in this investigation in terms of cut edge corrosion a 5 mm groove was machined into a section of material from the centre of each casting and a mild steel strip inserted into the groove thus allowing corrosion tests to be performed that mimicked cut-edge corrosion whereby anodic dissolution of the zinc alloy is driven through cathodic protection of the exposed steel. The microstructure of the material

either side of the steel insert was examined to ensure that the manufacture of the false cut-edge had not changed the structure in any way and also to ensure no crevices existed between the casting and insert and this was found to be the case for both the irradiated and un-irradiated castings. A schematic example of the sample prepared in this manner in shown in figure 2B. The portion of casting with a false cut-edge was then polished flat and to a mirror finish using progressively finer emery papers and 1 μm diamond slurry to ensure reproducible surfaces for SVET testing. The sample was then masked using PTFE tape to leave an area of 1.05×10^{-4} m^2 (105 mm^2) exposed for SVET experiments. The area was masked carefully to ensure a ratio of 1:5 in terms of exposed Zinc alloy to steel in order to simulate a cut-edge where generally the exposed area of steel is much larger than Zn alloy coating. For each test the area scanned by the SVET was 15 mm along the false cut edge and 7 mm perpendicular to this, across the edge ensuring both steel. Examples of scan areas are shown in figure 2B. The SVET probe made 100 measurements along the length of the cut edge and 50 measurements across the samples width generating a matrix of 5000 data points for each scan. Three areas of each casting were scanned namely the top, which was closest to the point of application of the ultrasound probe (5 mm from horn), the middle (25 mm from horn) and the bottom (45 mm from horn) to assess the effect of distance from horn on corrosion resistance. These areas are shown in figure 2B. The SVET tests were carried out in 0.1% NaCl solution and one scan was taken every hour for 24 hours and three repeat tests for each material were carried out. The dissolved oxygen concentration in bulk solution was assumed to be constant at 0.28 mol m^{-3}, the equilibrium concentration for air saturated water, thus promoting oxygen reduction as the dominant cathodic reaction. All tests were carried out at 25^{o}C.

2.3.1 SVET apparatus and calibration

The SVET has been readily used in the investigation of cut edge corrosion in zinc coated and organically coated steels with much success [17-25]. The SVET probe used in the investigation was a 125 μm diameter Platinum wire micro-tip encased in glass. The probe was mechanically vibrated by an EG & G 7625 lockin amplifier at a constant frequency of 140 Hz, an amplitude of 25 μm and at a constant height of 100 μm above the corroding surface immersed in 0.1% NaCl. The probe detects an alternating potential at the vibration frequency that is proportional to the potential gradient in solution in the vibration direction. Potential gradients in solution are established by ionic current fluxes generated above corroding surfaces and hence the SVET can provide important spatial and time resolved mechanistic information as to the location and intensity of anodes and cathodes on metals immersed in electrolyte. The apparatus and operation of the technique has been fully described elsewhere [25]. The potential gradients detected by the SVET probe in solution are measured in nV and the SVET was calibrated prior to each experiment to convert these measured voltages to current density, Am^{-2}. This was achieved by exposing the SVET probe to various uniform current densities and measuring its voltage response to produce a plot of current density versus SVET measured voltage. This calibration was achieved using a two compartment cell and a full description of the methodology is presented in previous research [25]. The two compartment cell provides a rapid and height independent method of calibrating the SVET before each experiment. The gradient of a plot of current density versus SVET voltage provides a calibration factor for the instrument with a typical value in 0.1% NaCl being 15,000 Am^{-2} V^{-1}.

2.3.2 Manipulation of SVET data

The data recorded by the SVET can provide a semi-quantitative estimate of metal loss over time from a sample through the integration of positive current data and the application of

Faraday's law. This manipulation of data is very useful when comparing similar materials such as Zn coated steels with different alloy coatings or processing conditions. The theory behind the calculations to achieve this mass loss has been presented elsewhere [25]. The metal loss data is semi-quantitative due to a number of assumptions [25] made in the calculations and thus these data should not be used as an absolute measure of the samples mass loss. However, in previous research the use of SVET data in this way has provided reliable predictions of the performance and metal loss from various Zn coated steels when compared with long term external weathering [17,18,24].

The SVET data can be further manipulated to locate, measure and track the position of anodic events above a defined current density threshold of 1 Am^{-2} over the duration of the experiment. This was achieved by developing a Visual Basic macro that interrogated the matrix of SVET data for each hourly scan to locate the positions of anodes and then track them over the 24 hour experiment. The lifetime and intensity of each anodic feature could then be monitored providing a valuable insight into the corrosion behaviour of a material and the influence of its microstructure on corrosion.

3.0 Results and Discussion

3.1 Solidification of Zn - 4.8 wt.% Al alloys as predicted by the phase diagram.

The Zn - 4.8wt.% Al alloy under investigation lies just to the right of the eutectic point of 5 wt.% Al in the Zn/Al equilibrium phase diagram as shown in the schematic in figure 3. On cooling from the liquid phase through the liquidus line nucleation of η crystals of primary Zn occurs at some undercooling below the liquidus temperature and the remaining liquid ahead of the solidification front becomes enriched in Al. As cooling proceeds the η crystals start to grow into a dendritic structure under practical cooling rates and when the remaining liquid

reaches 5 wt.% Al it solidifies into a lamellar eutectic of alternating sheets of η Zn and β Al [26]. A rod eutectic can form but generally at very high cooling rates, around the primary dendrites due to orientation effects or with small additions of ternary elements such as Mg. The final microstructure is therefore composed of primary zinc dendrites in a matrix of lamellar Zn/Al eutectic.

3.1.1 Microstructure morphology of cast Zn – 4.8wt.% Al alloys with no ultrasonic irradiation and with ultrasonic irradiation

Figure 4 shows macro digital camera images of sectioned casts of Zn – 4.8 wt.% Al alloy having had no ultrasound during solidification, figure 4A and having ultrasonic irradiation during solidification, figure 4B. Figure 4 shows that the sample that had experienced irradiation had a much finer grain structure below the position of the ultrasound horn and this structure extended throughout the casting vertically and laterally to the chill zone. The casting that had no ultrasound had a much larger grain structure throughout the suggesting that the ultrasound had a significant impact on the solidification of the alloy.

An optical microscope image of the Zn – 4.8wt.% Al alloy without ultrasonic irradiation is shown in figure 5A. The microstructure was composed of primary dendrites in a lamellar eutectic matrix as predicted from the phase diagram. EDX and XRD analysis is presented in figures 6A and 7. The EDX analysis in figure 6A showed that the primary dendrites were composed of 97.1 wt.% Zn, 1.8 wt.% Al and 1.1 wt.% Fe whilst the eutectic regions had a composition with an increased wt. % of Al of 91.8 wt.% Zn, 7.1 wt.% Al and 1.1 wt.% Fe. These data would seem to conform to the solidification theory outlined in section 3.1 where the primary dendritic phase was predicted to be Zn rich surrounded by a Zn / Al eutectic

matrix. The presence of Fe was a result of the alloy spelter being taken from the process galvanising bath that is saturated with Fe due to the constant movement of steel strip through it. The XRD data for the sample with no ultrasound provided in figure 7 showed a crystalline structure and peak identification through comparison to previous research on this alloy enabled the identification of η Zn and β Al phases as the predominant structures in the sample [27]. The EDX and XRD data presented support previous research into similar alloys [26, 27, 28] that the microstructure was composed of primary Zn rich η dendrites surrounded by a eutectic of η Zn / β Al as described in section 3.1. The eutectic structure was primarily of lamellar morphology with alternating lamellae of η Zn and β Al with some pockets of rod eutectic observed next to primary and secondary dendrite arms of the Zn rich η phase. The formation of rod eutectic next to the dendrite arms was most likely as a result of lamellae becoming forced to growth at orientations away from the preferred growth direction as shown by previous research [29, 30]. Figure 5B shows an optical microscope image of the typical microstructure of the cast Zn – 4.8wt Al alloy that was ultrasonically irradiated. EDX and XRD analysis is presented in figures 6B and 7. The EDX analysis in figure 6B was very similar to the sample with no ultrasound with the primary dendrites composed of 97.6 wt.% Zn, 1.4 wt.% Al and 1.0 wt.% Fe whilst the eutectic regions had a composition of 90.5 wt.% Zn, 8.4 wt.% Al and 1.1 wt.% Fe. The XRD analysis of the ultrasound sample, shown by the dotted trace in figure 7, was also practically identical to the sample with no ultrasound with peak analysis showing the presence of η Zn and β Al. Thus it can be concluded that the ultrasonic irradiation had little or no effect on the Zn or Al phases formed as the microstructure was again the structure characterised by a Zn rich η phase and a η Zn / β Al eutectic. However, there were significant morphology changes compared with the casting produced without ultrasonic irradiation. The primary Zn rich η phase was predominantly globular with no obvious dendritic structures visible compared with the non-irradiated

sample. The majority of the eutectic structure was still lamellar but there were significant areas where the eutectic growth had become disrupted forming almost spherical colonies of anomalous eutectic growth. These regions of anomalous eutectic were often characterised by numerous primary η globules at their periphery. The microstructures of both castings were compared at distances up to 40 mm from the position of the ultrasound horn along the centreline of the castings. The change from dendritic primary η phase to globular was evident when comparing the non-irradiated and irradiated sample images at all distances up to 40 mm from the horn. No dendritic structures were observed in over 140 images taken of the irradiated sample suggesting a shift away from dendritic growth.

For all images, the number of primary η phase crystal regions per mm^2 was evaluated for each alloy condition as a function of distance away from the ultrasound horn. These η regions may reflect individual dendrites or dendrite arms co-incident with the plane of the image or individual globular η crystals. These data are presented in figure 8. It can be clearly seen that there is a significant increase in the number of primary η crystal regions per mm^2 when ultrasound is applied during solidification at all distances considered and this is especially prominent over the first 20 mm away from the horn. At 5 mm from the horn there were almost 60 primary η crystal regions observed mm^{-2} for the ultrasound sample compared with 1 primary η crystal region mm^{-2} for the sample with no ultrasound. In the sample with no ultrasound this low number of primary crystal regions at the centre of the casting close to the top represents the last liquid to solidify and this will be of eutectic composition so there will be relatively few if any primary η crystals. The conditions imparted by the ultrasound thus seem to allow enhanced nucleation of primary η phase throughout the solidification. At distances greater than 20 mm there is a marked increase in primary η crystal regions mm^{-2} in

the no ultrasound sample rising from < 20 mm^{-2} at 1.5 mm to a fairly stable 60 mm^{-2} at distances > 20 mm.

The instantaneous volume fraction of primary η phase for each image was evaluated as a function of distance from the horn for samples with no ultrasound and with ultrasound. The results are shown in figure 9. The major differences were observed over the first 20 mm from the ultrasound horn with a significant increase in volume fraction of primary η phase in this area of the casting when ultrasound was applied. The volume fractions of primary phase at distance > 20 mm from the horn were fairly similar with a typical value of around 17% primary η phase for both casting conditions but overall there was an increase from 10% to 15% in the overall average volume fraction of primary η phase when ultrasound was applied. The application of the ultrasound produced a more even distribution of primary η phase throughout the casting whereas there is significant non-uniformity of primary η volume fraction with distance from the horn when no ultrasound was applied. These instantaneous volume fraction data and the number of primary η crystal regions mm^{-2} were then used to calculate an average size of the primary crystal regions (mm^2) as a function of distance from the horn for both castings and are presented in figure 10. These data show that the average size of regions of η primary crystal in castings exposed to ultrasound varied between a minimum of 1.1 x 10^{-3} mm^2 at 5 mm and a maximum of 1.7 x 10^{-3} mm^2 at 40 mm from the horn. For the sample with no ultrasound the average size of η primary regions varied between a minimum of 1.4 x 10^{-3} mm^2 at 15 mm and a maximum of 2.99 x 10^{-3} mm^2 at 25 mm from the horn. Thus, considering figures 9 and 10, the application of ultrasound produced an overall increase in the volume fraction of primary η whilst individual primary phase regions were consistently smaller when ultrasound was applied and maintained a more uniform size throughout the casting.

Figures 8 – 10 thus demonstrate that the application of ultrasound to the solidifying Zn – 4.8 wt.% Al alloy has a significant influence on the final microstructure. The ultrasound samples are generally characterised by a small, globular primary η phase regions with an increase in the volume fraction of this phase. The eutectic structure is also altered with areas of disruption of stable planar eutectic growth forming colony like structures of anomalous eutectic as shown in figure 5C. Ultrasound creates a unique environment within the melt on irradiation. The Ultrasound waves create areas of compression and rarefaction within the melt that leads to the formation of cavitation where the melt is literally torn apart by the vibration creating a cavity. These cavities are generally unstable and collapse in on themselves which causes large local temperature and pressure increases. In fact locally temperatures may reach 5000^{o}K and several hundred atmospheres of pressure [11]. The ultrasound waves also move through the melt in a phenomenon known as acoustic streaming that can cause rapid agitation and mixing and can influence convective heat flow. The cavitation phenomenon can also aid degassing of melts and removal of gas from the surfaces of intermetallic /oxide inclusions thus potentially providing suitable surfaces for nucleation events [1].

The transition of the primary Zn rich η phase from dendritic to globular on application of ultrasound may be due to a number or combination of factors. Dendritic growth is caused by compositional variations along a solidifying interface that cause protrusions to grow from a planar interface. In terms of ultrasonic irradiation the mixing and flow of liquid induced by acoustic streaming and local cavitation events may offer sufficient stirring to rapidly remove solute build up ahead of growing interfaces. This homogenising of the liquid ahead of the solidification front would therefore promote stability of the planar interface by removing constitutional supercooling effects and thus prevent the formation of stable dendrite arms

producing globular primary crystals of η. The fluid dynamics induced by the ultrasound may also have the effect of fragmenting dendrites that form in the melt by breaking off any secondary arms that form due to forces induced by acoustic streaming and cavitation [31]. This would then produce a final microstructure of globular primary η as the dendrite arms are removed. It would also contribute to the observed increase in primary η crystal regions as each arm removed would form a "stand alone" crystal in its own right. Acoustic streaming induced fluid flow may also disrupt dendrite formation through the bending of secondary dendrite arms that would induces stresses at the root of the arms. This stress would cause localised heating of the root and if close to the liquidus temperature could cause re-melting of the root and subsequent detachment of the arm [32]. It is extremely difficult to prove which of these effects has a dominant role in the breakdown of dendritic growth due to the difficulty of monitoring microscopic solidification in such an extreme environment. However, Figure 9 demonstrates that there was much improved mixing when ultrasound was applied to the melt as the volume fraction of primary η is much more even throughout the casting with only a small eutectic rich area just below the ultrasonic horn extending to 5 mm whereas a stable volume fraction was not achieved until a depth of 25 mm in the sample cast without ultrasound. This implies that the liquid was mixed more thoroughly achieving a more homogenous mix and that local compositional differences during solidification were rapidly removed.[1,2,3].

The eutectic structure in the non-ultrasound samples is primarily lamellar with alternating sheets of Zn and Al as shown in figure 5A. Some rod eutectic is formed around the secondary dendrite arms where preferred orientation growth is disrupted by the dendrite arms [29,30]. Lamellar eutectic formation is associated with lateral diffusion of Al from growing phases of Zn and vice versa in a process known as coupled growth that allows lamellae of each phase to

grow concurrently and adjacent to each other. Examination of figures 5B and 5C for the Zn – 4.8wt.% Al alloy solidified with ultrasound shows that although the regular lamellar Zn/Al was still present there were also numerous, almost spherical colonies of anomalous eutectic growth. The regions of anomalous eutectic are intriguing and demonstrate a region where solidification conditions have changed locally to breakdown the stable lamellar growth. Stable planar growth resulting in a lamellar structure is promoted by a low growth rate, a steep temperature gradient ahead of the growth front and the absence of mixing due to the need for short-range diffusion. Thus, ultrasonic irradiation seems to have disrupted these conditions in a localised fashion. At the point of eutectic solidification cavitation effects within the melt will be reduced due to the mushy conditions and so other factors such as acoustic streaming must influence this change in morphology.

3.2 Corrosion behaviour of Zn – 4.8wt.% Al alloys solidified with and without ultrasound as determined by the SVET

Both castings of Zn – 4.8 wt.% Al alloys with and without ultrasonic irradiation during their solidification have been prepared as described in section 2.3 for corrosion testing using SVET. The samples were prepared to give false cut edges to mimic in-service coating conditions and three areas on the castings were scanned to assess the effect of distance from the ultrasonic horn on the change in microstructures effect on corrosion resistance as shown in figure 2B. Figure 11 shows typical 3D current density maps for samples A) without ultrasound B) with ultrasound. The maps were plotted in Surfer 10 (Golden Software). The 3D maps show areas of anodic activity as positive current density peaks and areas of cathodic activity as negative current density troughs. The current density maps show that anodic activity was focussed towards the edges of the scan area where the Zn – 4.8wt.% Al alloy

was exposed. The centre portion of the scan was persistently cathodic over the steel insert thus confirming that the alloy was sacrificially protecting the steel as per an in service cut-edge of production material. At the anode Zn dissolves as shown in equation 1 and at the cathode the steel provides a site for cathodic oxygen reduction, equation 2.

$$2Zn \rightarrow 2Zn^{2+} + 4e^{-} \quad (1)$$

$$2H_2O + O_2 + 4e^{-} \rightarrow 4OH^{-} \quad (2)$$

There were generally a greater number of anodic peaks observed on samples tested that were solidified with ultrasonic irradiation. This persisted from scan to scan for the top and middle (5 mm and 25 mm from the horn) scan areas interrogated on each casting with a false cut edge. A similar number of anodes were observed for both castings at the bottom scan position (45 mm from the horn).

SVET measured Zn loss data (as described in section 2.3.2) is presented in figure 12 for both alloys at the three distances from the ultrasonic horn. The data presented in figure 12 represents an average of three tests for each experimental condition and the error bars reflect the limits of these data observed. It can be seen from figure 12 that the samples that experienced ultrasonic irradiation during solidification generally outperformed the non-ultrasound samples at all positions through the casting in terms of SVET measured Zn loss. This may therefore be of potential interest for the steel manufacturer. It is intriguing that the data in figures 11 and 12 seem contradictory in that the ultrasound sample that had more anodic features had a lower overall metal loss than the casting with no ultrasound. It is thus important to look at the lifetime of anodes that develop over the course of 24 hours as longer living anodes at any one site will be more damaging than short lived anodes especially if they

maintain a relatively high current density. This means that a few long lived anodes can be more damaging than numerous short lived anodic events. Figure 13 shows the percentage of anodes that are active for defined time frames, 0-6 hours, 6-12 hours, 12-18 hours and 18-24 hours for both alloy preparation conditions. The graph shows that for both the top and middle scan positions (5 mm and 25 mm from the ultrasonic horn) the sample irradiated with ultrasound showed a reduction in anodes that had the longest lifetimes i.e. those having an intensity of greater than 1 Am^{-2} for 18 – 24 hours of the experiment time. These are the most damaging anodes in terms of metal loss and hence this may explain the reduction in corrosion rate observed.

These data suggest that the change in microstructure induced by ultrasound imparts an improved corrosion performance on the Zn – 4.8 wt.% Al alloy at cut-edges. Previous work has shown that the size of the primary Zn rich η dendritic phase is critical in determining corrosion behaviour of this alloy and modifications of the dendrite size through cooling rate, coating thickness or steel substrate thickness can significantly influence the corrosion performance of the alloy [17, 18, 25]. When cut edge corrosion occurs and the Zn alloy acts to protect the steel, anodic activity becomes focussed on the Zn rich η phase preferentially. This is shown in figure 14 where localised corrosion of the η phase was observed on examination of the corroded alloy that was solidified with ultrasound after immersion in 0.1% NaCl in the SVET experiments. Figure 15 shows that for the alloy sample irradiated with ultrasound during solidification there is a general trend between the number of primary η regions per mm^2 and the average primary η region size with the SVET measured Zn loss suggesting that indeed η morphology was a controlling factor for anodic dissolution rate. Figure 15 also shows that for the non-ultrasound sample the trend holds for the middle and bottom areas considered during the SVET testing but the top portion of the casting is

predominantly eutectic in this sample and thus the relationship breaks down. Here, the corrosion may involve de-alloying of the Zn rich lamellar from the eutectic phase driven ultimately by the cathodic activation of the steel insert. Thus, it would seem that the application of ultrasound on solidification reduces the corrosion rate of the alloy through morphological changes to the primary η phase. As this phase is the focussed point for anodic attack the modification to smaller, more numerous primary η regions reduces the corrosion rate as these smaller primary crystals provide sites for anodes with shorter lifetimes and are less likely to develop into deeper crevice like features that may be seen with larger η features. Larger primary η regions may support longer living anodes and as metal is excavated through the anodic process, localised aggressive chemical conditions may occur that could expedite the corrosion processes in the region local to the dendrite hence increasing the corrosion rate.

4.0 Conclusions

The application of ultrasound to the solidifying melt of Zn – 4.8wt % Al alloys significantly altered the morphology of the final microstructure and also influenced the cut edge corrosion behaviour as evidenced through SVET for simulated coated steel samples. Samples irradiated with ultrasound had smaller primary η phase crystal regions mm^{-2} but with an increased volume fraction. The ultrasound sample also demonstrated a much more uniform distribution of primary phase with a stable volume fraction of η observed throughout the casting in comparison to the non-ultrasound sample. The morphology of the phases within the microstructure were altered with the application of ultrasound from dendritic to globular primary η and in localised areas from lamellar to anomalous eutectic. These changes were apportioned to the physical action of the ultrasound possibly causing the fragmentation of dendrites and disruptive compositional effects that led to the breakdown of constitutional supercooling and coupled eutectic growth.

The change in microstructure morphology induced by ultrasound had a generally positive effect on the corrosion behaviour of the alloy in 0.1% NaCl when investigated in the SVET. A steel insert was incorporated into the samples to create a false cut-edge thus mimicking in service conditions when the alloy is used as a coating on steel. The primary η crystals were the focussed sites for anodic dissolution and the smaller primary η crystals induced by the ultrasound reduced the corrosion rate by preventing the establishment of crevice like phenomena that may be associated with larger dendritic features. This was demonstrated by a reduction in lifetimes of anodic features on the ultrasound samples. It was also shown that changes in primary η region numbers and size generally influenced the corrosion rate with reductions in these factors subsequently reducing the corrosion rate of the alloy.

5.0 Acknowledgements

The Authors wish to thank TATA Steel Shotton Works, Deeside for access to the Galvanising facilities to carry out the initial experiments and the EPSRC for CASE award funding for Dr Khan. We would also like to thank Lewis Berry and Tom Lewis of Swansea University for their assistance with XRD and EDX.

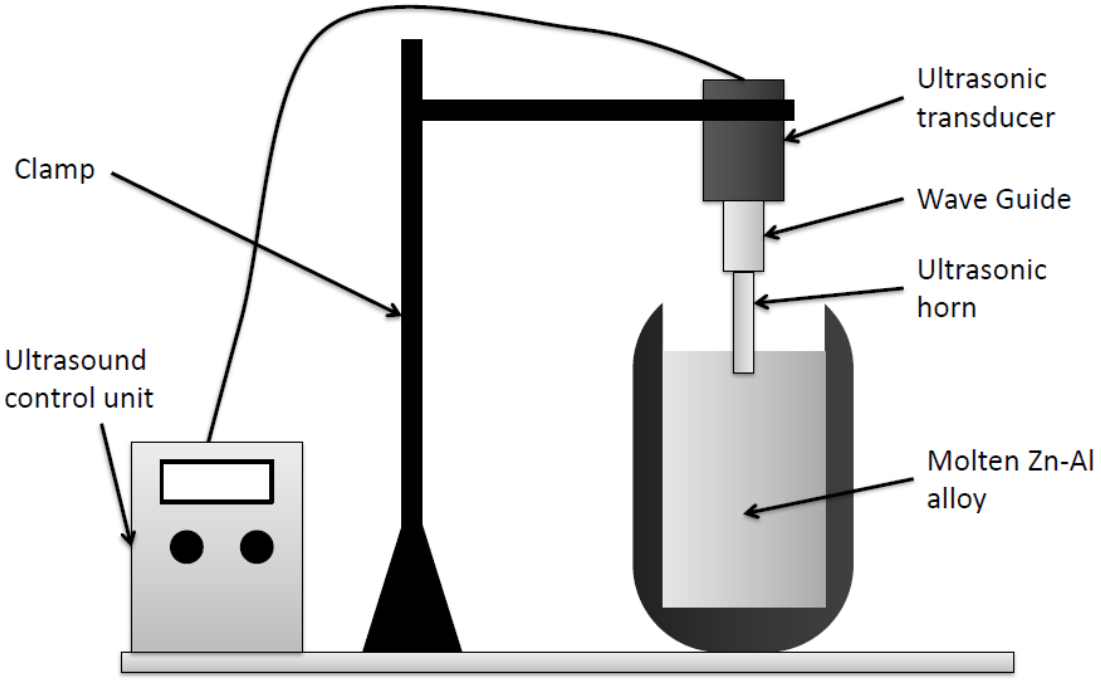

Figure. 1

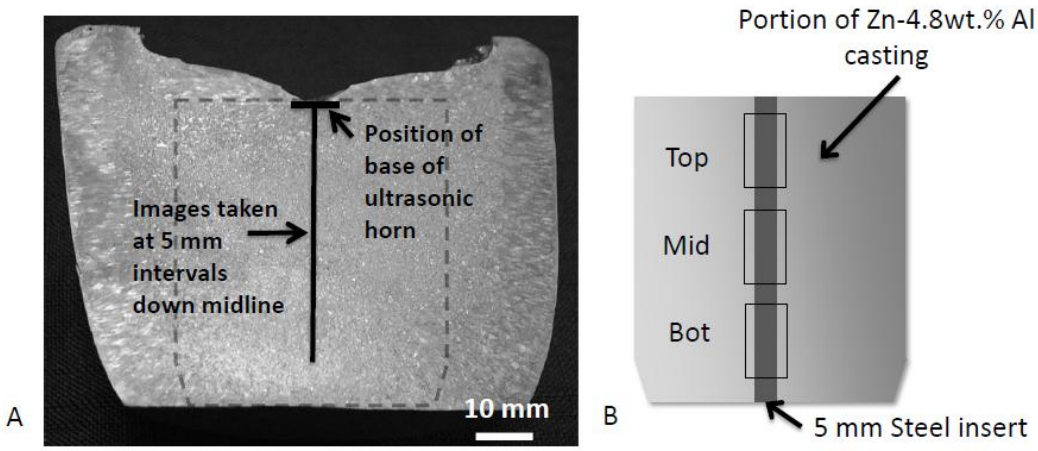

Figure. 2

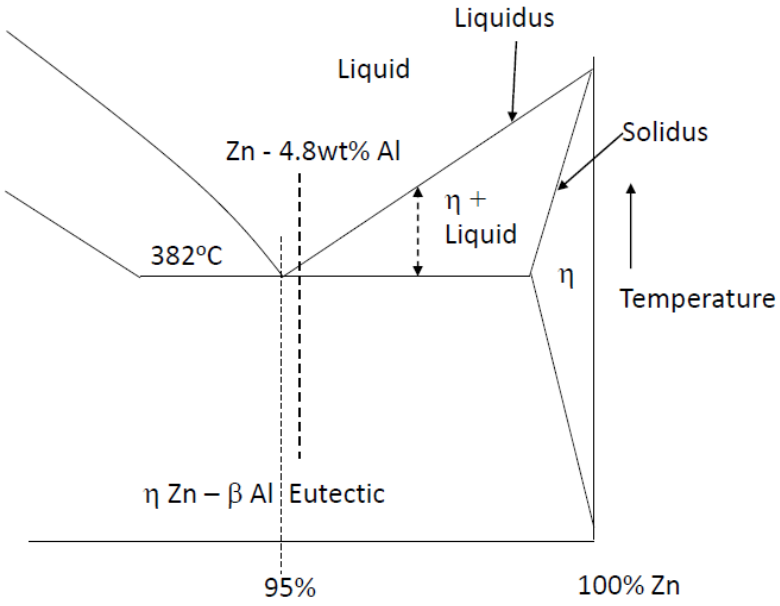

Figure 3

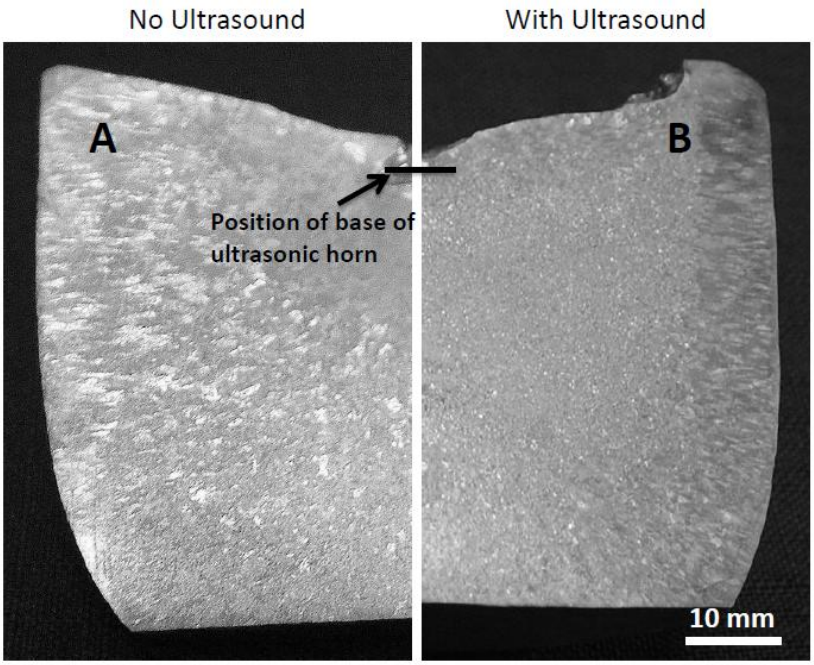

Figure. 4

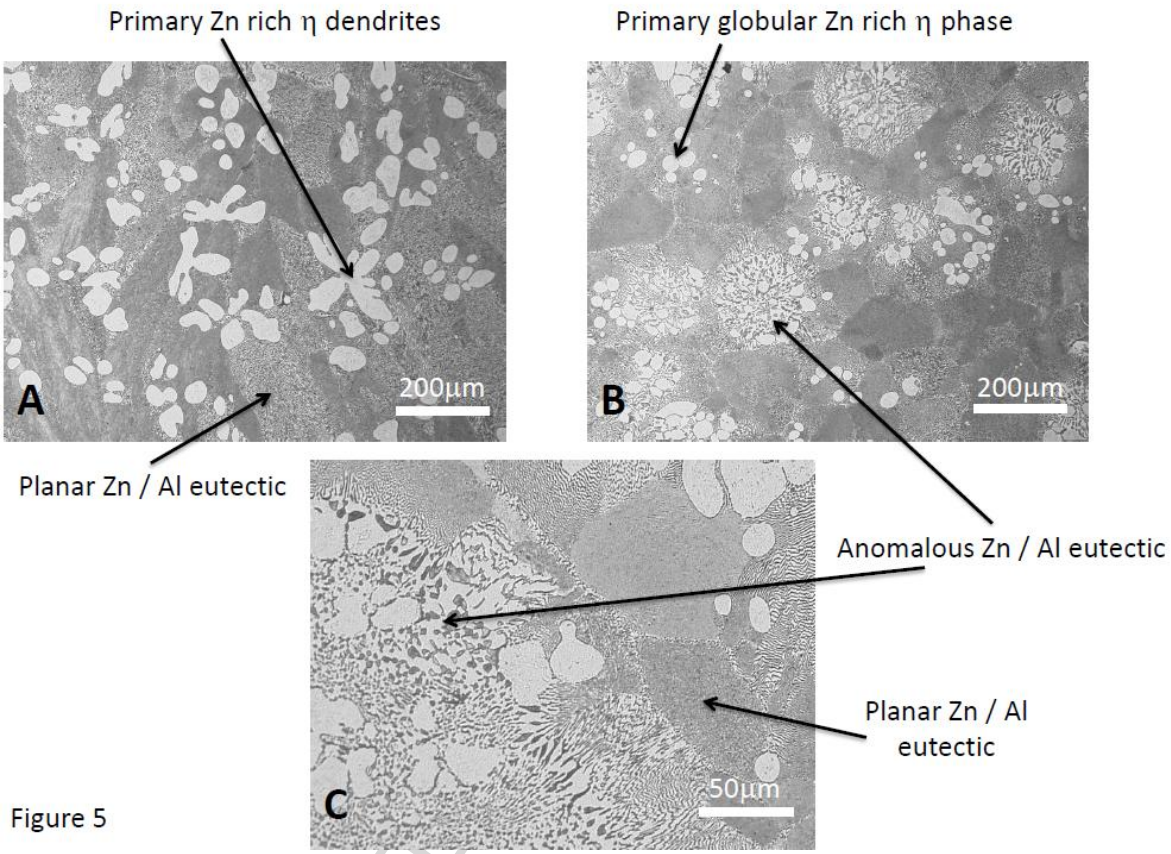

Figure 5

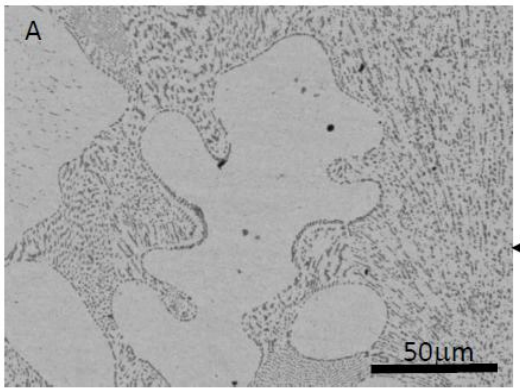

No Ultrasound		
Element	Dendrites (wt.%)	Eutectic (wt.%)
Zn	97.1	91.8
Al	1.8	7.1
Fe	1.1	1.1

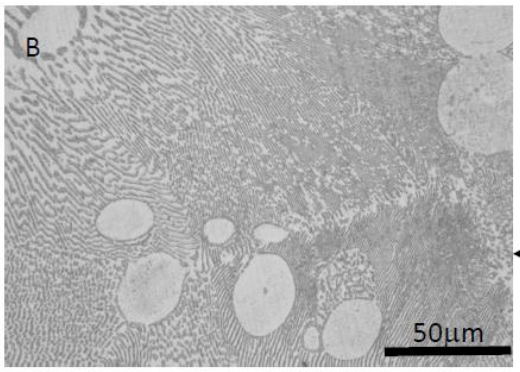

Ultrasound		
Element	Dendrites (wt.%)	Eutectic (wt.%)
Zn	97.6	90.5
Al	1.4	8.4
Fe	1.0	1.1

Figure 6

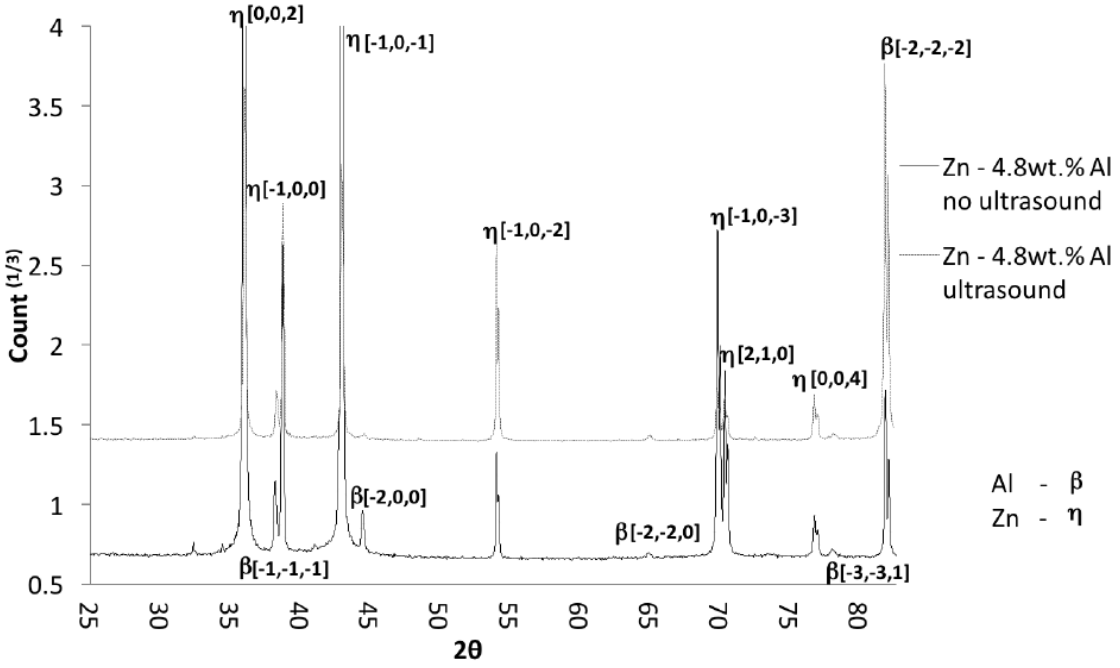

Figure 7

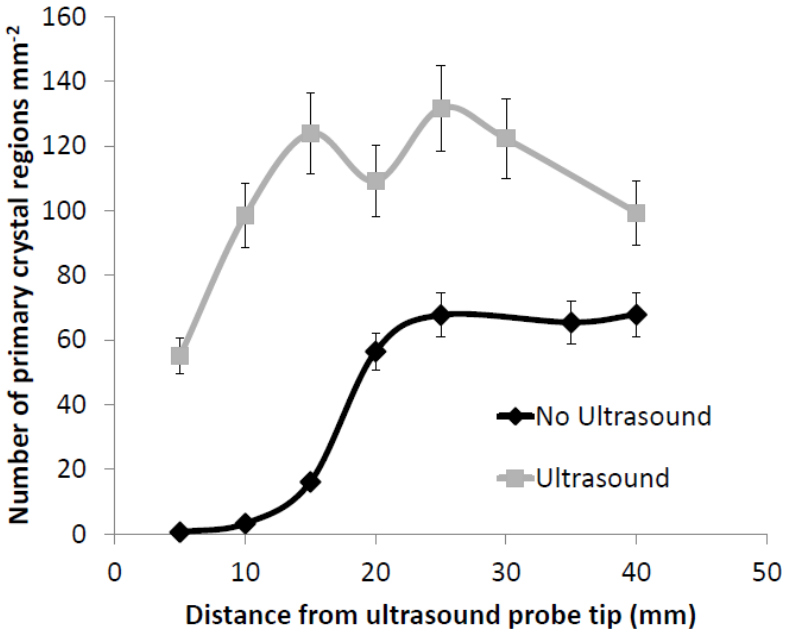

Figure. 8

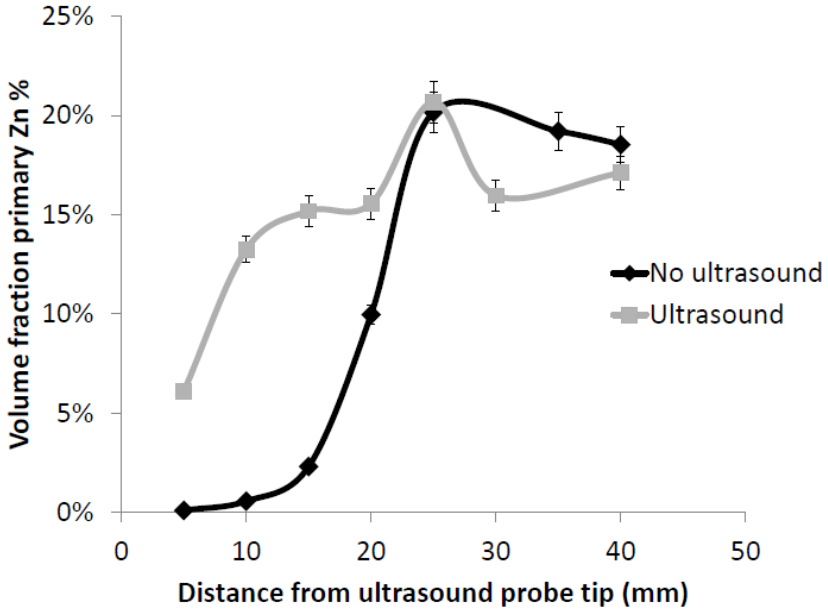

Figure. 9

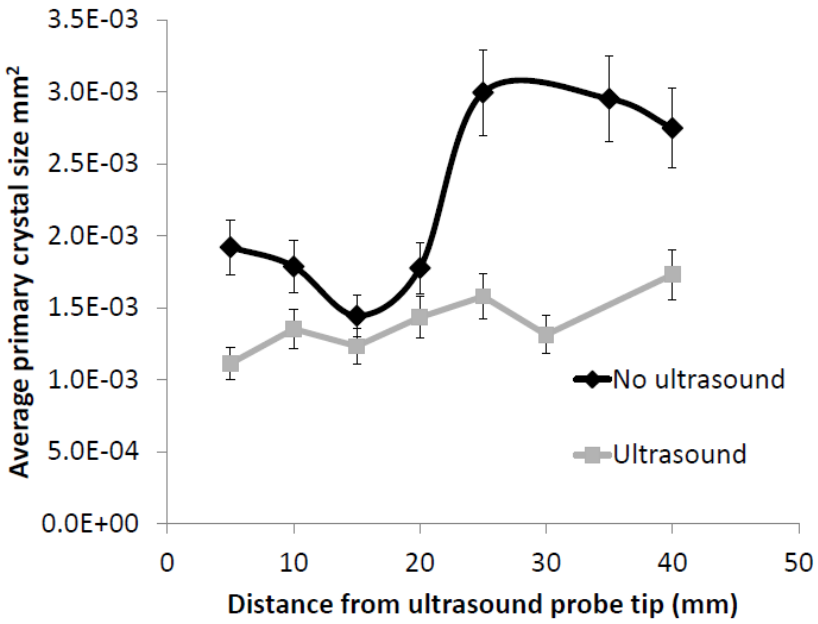

Figure. 10

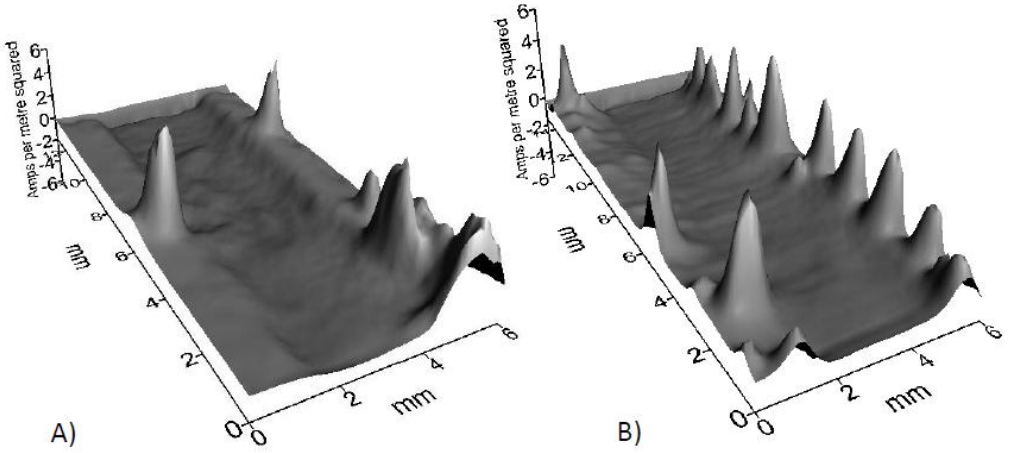

Figure. 11

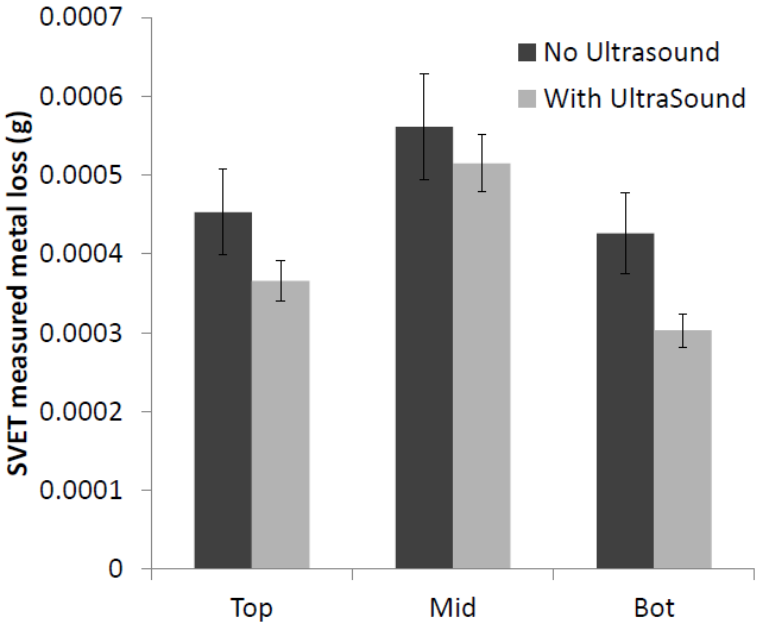

Figure. 12

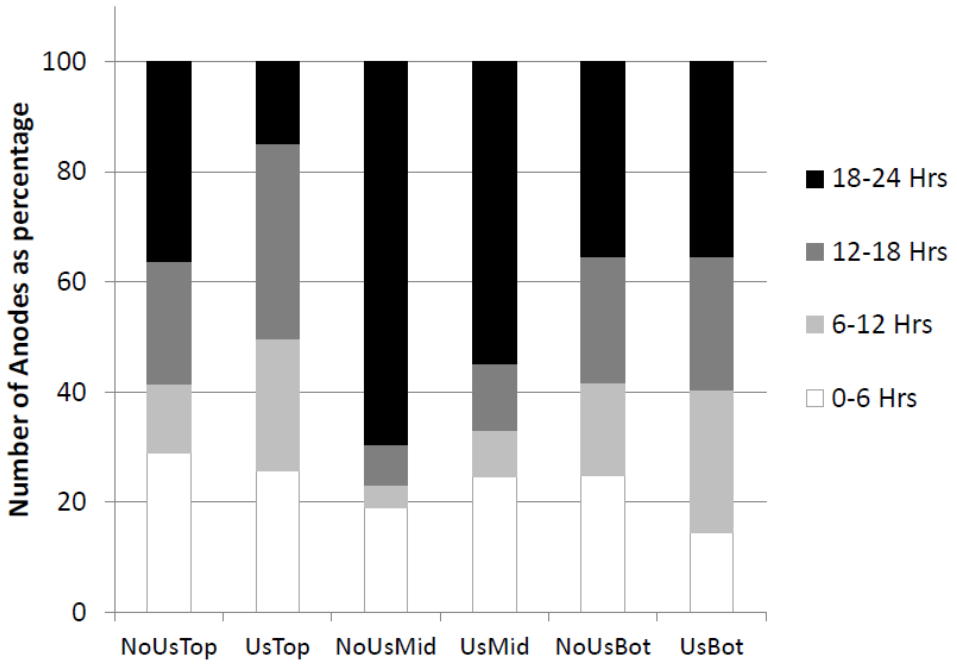

Figure. 13

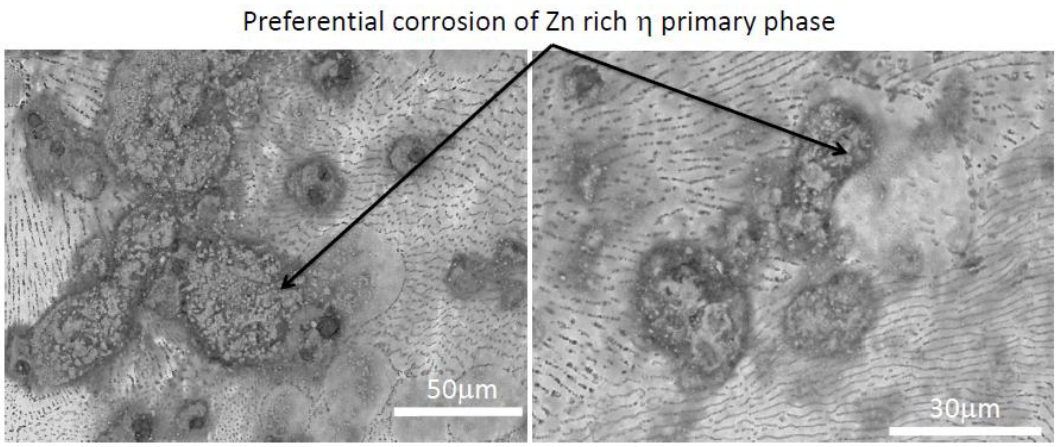

Figure. 14

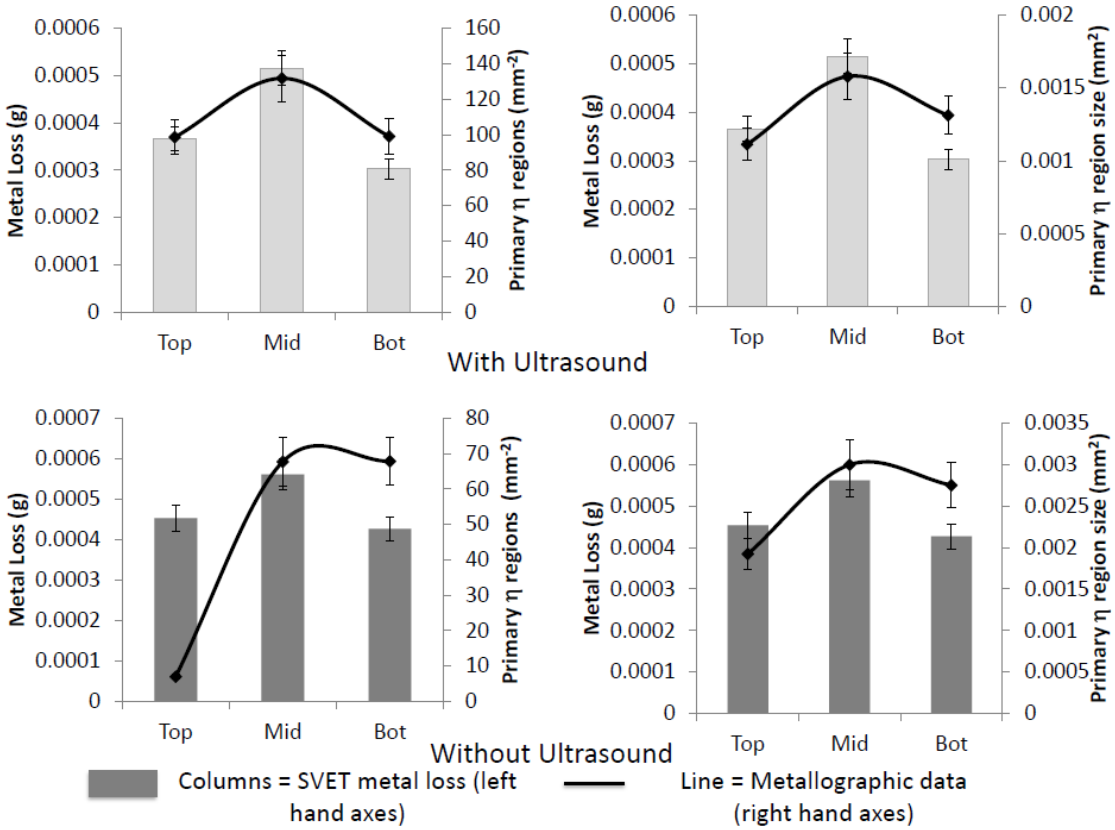

Figure. 15

The effect of ultrasonic irradiation on the microstructure and corrosion rate of a Zn – 4.8 wt% Al galvanising alloy used in high performance construction coatings

Research Highlights

1) Microstructures of Zn/Al galvanising alloys are modified by ultrasound during solidification
2) Morphology of primary η Zn and Zn/Al eutectic phases are altered significantly
3) Volume fraction of primary η Zn increased by ultrasound
4) Galvanic corrosion resistance of the ultrasound treated Zn/Al alloy is improved
5) Morphology of primary η Zn phases in microstructure influence corrosion rate

References

[1] G.I. Eskin, Broad prospects for commercial application of the ultrasonic (cavitation) melt treatment of light alloys, Ultrason. Sonochem, 8 (2001) 319-325

[2] G.I. Eskin, Cavitation mechanism of ultrasonic melt degassing, Ultrason. Sonochem, 2 (1995) 137-141

[3] G.I. Eskin, G.S. Makarov, Y.U.P. Pimenov, Effect of ultrasonic processing of molten metal on structure formation and improvement of properties of high-strength Al-Zn-Mg-Cu-Zr alloys, Adv. Perform. Mater, 2 (1995) 43-50

[4] V. Abramov, O. Abramov, V. Bilgakov, F. Sommer, Solidification of aluminium alloys under ultrasonic irradiation using water-cooled resonator, Mater. Lett, 37 (1998) 27-34

[5] H. Yanfen, L. Ke, W. Jun, S. Da, S. Baode, Influence of high-intensity ultrasound on grain refining performance of Al–5Ti–1B master alloy on aluminium, Mat. Sci. Eng. A, 405 (2005) 306-312

[6] Z. Zhongtao, L. Tingju, Y. Honyun, Z. Jian, L. Jie, Study on the preparation of Al–Si functionally graded materials using power ultrasonic field, Mater. Design, 30 (2009) 851-856

[7] H.K. Feng, S.R. Yu, Y.L. Li, L.Y. Gong, Effect of ultrasonic treatment on microstructures of hypereutectic Al–Si alloy, J. Mater. Process. Tech, 208 (2008) 330-335

[8] A. Soare, R. Dijkink, M.R. Pascual, C. Sun, P.W. Cains, D. Lohse, A.I. Stankiewicz, H.J.M. Kramer, Crystal Nucleation by Laser-Induced Cavitation, Cryst. Growth. Des. 11 (2011) 2311-2316

[9] D. Gao, Z. Li, Q. Han, Q. Zhai, Effect of ultrasonic power on microstructure and mechanical properties of AZ91 alloy, Mat. Sci. Eng. A. 502 (2009) 2-5

[10] J. Li, W. Chen, Q. Liu, X. Wang, Effect of ultrasonic treatment on the solidification structure of high carbon steel containing rare earth elements, Steel. Res. int, 79 (2008) 358-363

[11] A. Ramirez, M. Qian, B. Davis, T. Wilks, D.H. StJohn, Potency of high-intensity ultrasonic treatment for grain refinement of magnesium alloys, Scripta. Mater. 59 (2008) 19-22

[12] M. Qian, A. Ramirez, A. Das, Ultrasonic refinement of magnesium by cavitation: Clarifying the role of wall crystals, J. Cryst. Growth. 311 (2009) 3708-3715

[13] X. Jian, H. Xu, T.T. Meek, Q. Han, Effect of power ultrasound on solidification of aluminum A356 alloy, Mater. Lett. 59 (2005) 190-193

[14] D.G. Eskin, M. Faraji, L. Katgerman, Grain refinement in hypoeutectic Al-Si alloys using ultrasonic vibrations, Int. Foundry. Res. 62 (2010) 20-25
[15] T.V. Atamanenko, D.G. Eskin, L. Zhang, L. Katgerman, Criteria of grain refinement induced by ultrasonic melt treatment of aluminum alloys containing Zr and Ti, Metal. Mater. Trans. A. 41 (2010) 2056-2066
[16] L. Zhang, D.G. Eskin, L. Katgerman, Influence of ultrasonic melt treatment on the formation of primary intermetallics and related grain refinement in aluminum alloys, J. Mater. Sci. 46 (2011) 5252-5259
[17] J. Elvins, J.A. Spittle, D.A. Worsley, Microstructural changes in zinc aluminium alloy galvanising as a function of processing parameters and their influence on corrosion, Corros. Sci. 47 (2005) 2740-2759
[18] D.J. Penney, J.H. Sullivan, D.A. Worsley, Investigation into the effects of metallic coating thickness on the corrosion properties of Zn–Al alloy galvanising coatings, Corros. Sci. 49 (2007) 1321-1339
[19] A.M. Simões, J. Torres, R. Picciochi, J.C.S. Fernandes, Corrosion inhibition at galvanized steel cut edges by phosphate pigments, Electrochim. Acta. 54 (2009) 3857-3865
[20] D.A. Worsley, D. Williams, J.S.G. Ling, Mechanistic changes in cut-edge corrosion induced by variation of organic coating porosity, Corros. Sci. 43 (2001) 2335-2348
[21] F. Thébault, B. Vuillemin, R. Oltra, K. Ogle, C. Allely, Investigation of self-healing mechanism on galvanized steels cut edges by coupling SVET and numerical modelling, Electrochim. Acta, 53 (2008) 5226-5234
[22] I.M. Zin, S.B. Lyon, A. Hussain, Under-film corrosion of epoxy-coated galvanised steel: An EIS and SVET study of the effect of inhibition at defects, Prog. Org. Coat. 52 (2005) 126-135
[23] A.C. Bastos, M.G.S. Ferreira, A.M. Simões, Comparative electrochemical studies of zinc chromate and zinc phosphate as corrosion inhibitors for zinc, Prog. Org. Coat. 52 (2005) 339-350
[24] J. Elvins, J.A. Spittle, J.H. Sullivan, D.A. Worsley, The effect of magnesium additions on the microstructure and cut edge corrosion resistance of zinc aluminium alloy galvanised steel, Corros. Sci. 50 (2008) 1650-1658
[25] J. Sullivan, C. Weirman, J. Kennedy, D. Penney, Influence of steel gauge on the microstructure and corrosion performance of zinc alloy coated steels, Corros. Sci. 52 (2010) 1853-1862

[26] A.R. Marder, The metallurgy of Zinc-coated steel, Prog. Mater. Sci. 45 (2000) 191-271
[27] M. Zelechower, J. Klis, E. Augustyn, J. Grzonka, D. Stróz, T. Rzychon, H. Woznica, The microstructure of annealed galfan coating on steel substrate, Arch. Metall. Mater. 57 (2012) 517-523
[28] X. Zhang, C. Leygraf, I. Odnevall Wallinder, Atmospheric corrosion of Galfan coatings on steel in chloride-rich environments, Corros. Sci. 73 (2013) 62-71
[29] K.A. Jackson, J.D. Hunt, Lamellar and rod eutectic growth, Trans. Metall. Soc. 236 (1966) 1129-1142
[30] F.R. Mollard, M.C. Flemings, Growth of composites from the melt: II, Trans. Metall. Soc. 239 (1967) 1534-1546
[31] A. Hellawel, S. Liu, S.Z. Lu, Dendrite fragmentation and the effects of fluid flow in castings, JOM 49 (1997) 18-20
[32] W.A. Tiller, S. O'Hara. The Solidification of Metals, The Iron and Steel Institute, London, 1968

Figure Legends

Figure 1. Schematic of apparatus used to ultrasonically irradiate the Zn - 4.8 wt.% Al melt

Figure 2. A - Cut face of section of casting polished to a 1 μm metallographic finish and etched. Dotted line represents section removed for corrosion testing post metallography. B - Portion of Zn - 4.8 wt.% Al alloy casting with steel insert to create a false cut-edge for corrosion testing with SVET. Testing carried out at three areas, Top, Mid(dle) and Bot(tom).

Figure 3. Schematic portion of Zn – Al equilibrium phase diagram showing the freezing characteristics of the Zn – 4.8 wt.% Al alloy

Figure 4. Macro digital camera images of sectioned casts of Zn – 4.8 wt.% Al alloy A) no ultrasound during solidification B) ultrasonic irradiation during solidification. The application of ultrasound produces a much finer microstructure throughout the alloy.

Figure 5 Optical micrographs of Zn – 4.8 wt.% Al Alloy solidified A) without ultrasound B) with ultrasound C) increased magnification image of eutectic phase for the sample irradiated

with ultrasound. The alloy shows a transition of primary η Zn phase from dendritic to globular and the formation of regions of anomalous Zn/Al eutectic on application of ultrasound.

Figure 6. EDX analysis of dendritic and eutectic regions for Zn – 4.8 wt.% Al alloy samples solidified without (A) and with (B) ultrasonic irradiation. The dendritic regions were predominantly Zn rich with an increased Al level observed in the eutectic regions of both samples. The compositions of the phases for both samples were very similar.

Figure 7. XRD diffractograms for Zn – 4.8 wt.% Al alloy solidified with and without ultrasound showing near identical peak profiles with the presence of crystalline η Zn and β Al phases in both samples.

Figure 8. The number of primary phase regions of η Zn per mm^2 evaluated as a function of distance away from the ultrasound horn showing a significant increase in η Zn regions for the sample irradiated with ultrasound during solidification.

Figure 9. Instantaneous volume fraction of primary η phase as a function of distance from the ultrasound probe tip for samples solidified with and without ultrasound. Samples with ultrasound had a more uniform volume fraction through the casting.

Figure 10. Average primary η region size (mm^2) as a function of distance from the ultrasound probe tip for samples solidified with and without ultrasound. The application of ultrasound promotes the formation of smaller η regions through the depth of the casting whereas a non-uniform distribution of sizes is produced without ultrasound.

Figure 11. Typical current density maps for Zn - 4.8wt.% alloys solidified A) without ultrasound B) with ultrasound, as detected with SVET in 0.1% NaCl. The ultrasound sample has more anodic peaks suggesting that microstructure modification has influenced the corrosion mechanism.

Figure 12. SVET determined Zn loss for both castings of Zn – 4.8wt.% Al alloy with a false cut edge for areas at various distances from the ultrasonic probe: Top – 5 mm, middle (Mid) – 25 mm, bottom (Bot) – 45 mm.

Figure 13. Percentage of anodes that are active for defined time frames, 0-6 hours, 7-12 hours, 13-18 hours and 19-24 hours for Zn - 4.8 wt.% Al alloys with and without ultrasonic irradiation during solidification.

Figure 14. Electron microscope images showing preferential corrosion of Zn rich η phase after immersion of Zn – 4.8 wt.% Al alloy in 0.1% NaCl for 24 hours.

Figure 15. Graphs showing effects of primary η crystal / dendrite morphology on the SVET measured Zn loss of Zn – 4.8wt.% Al alloys with a false cut edge solidified with and without ultrasound. In each graph corrosion metal loss is shown as columns with metallographic information as the line.